

# Experimental and Computational Evaluation of the Protection Provided by an Aluminum Cladding to AA2024-T3 Exposed at a Seacoast Environment

F. Cui,\* F.J. Presuel-Moreno,\* and R.G. Kelly<sup>†</sup>

## ABSTRACT

The effective throwing power of a common metallic cladding was investigated by analyses of samples of scribed Alclad, AA2024-T3 (UNS A92024), which were exposed outdoors at Daytona Beach, Florida, for between 2 months and 18 months. Both optical microscopy of the exposed plane surfaces and cross-sectional metallography were performed to assess the effects of scratch width on the level of protection afforded. For scratches 5 mm wide or smaller, the exposed AA2024-T3 substrates were generally well protected by AA1230 (UNS A91230) of the clad with only small corrosion pits, likely due to diurnal cycles that generated isolated electrolyte islands on exposed substrates. Conversely, for scratches between 6 mm and 10 mm wide, the exposed substrate was only partially protected by the clad, and the percentage of protection appeared to decrease with scratch size according to simple quadratic behavior. The clad exhibited significant pitting corrosion over its entire surface, independent of the size of the scratch. A computational framework was adapted to study the system described above. Computations showed that water layer thickness ( $WL$ ), scratch size,  $[Cl^-]$ , passive current density ( $i_p$ ) of clad, and diffusion-limited current density ( $i_{dl}$ ) of AA2024 all have a significant impact on the throwing power of clad. With  $[Cl^-] = 1\text{ M}$ ,  $WL = 25\ \mu\text{m}$ ,  $i_p = 0.002\text{ A/m}^2$ , and  $i_{dl} = 1.6\text{ A/m}^2$ , the model produced results that compared well to the experimental observations.

**KEY WORDS:** aluminum cladding, modeling, scratch, throwing power

## INTRODUCTION

Clad aluminum sheet consists of thin layers of near-pure aluminum that are metallurgically bonded to standard precipitation-hardened aluminum alloys. While the substrate provides mechanical strength, the aluminum coatings provide both physical and electrochemical protection for the substrate.<sup>1-2</sup> Such a unique integration of strength and corrosion performance has led to extensive applications of such materials (e.g., Alclad<sup>†</sup> AA2024-T3 [UNS A92024]<sup>[1]</sup>) in areas such as commercial and military aircraft fuselage skins, wing skins, and other aerospace structures.

A number of studies have confirmed good performance of Alclad after up to 30 years of field exposure and claimed protection of exposed substrate and edges adjacent to Alclad.<sup>1-4</sup> Generalizing such data is difficult as actual structures would have a range of damage sizes and would be subject to corrosiveness of different degrees depending on environmental factors and the geometry of the damage. Quantifying the throwing power of such claddings and identifying the controlling parameters is important for corrosion prediction modeling and cladding development. Because the restricted mass transport inherent in atmospheric corrosion conditions makes galvanic interactions between the cladding and any exposed substrate more difficult, this issue is of particular importance in aerospace applications. Systematic studies of the throwing power of Al claddings in such systems, however, have not been reported in the open literature.

Submitted for publication June 2005; in revised form, August 2005.

<sup>‡</sup> Corresponding author. E-mail: rgkelly@virginia.edu.

\* University of Virginia, Department of Materials Science and Engineering, 116 Engineer's Way, PO Box 400745, Charlottesville, VA 22903.

<sup>†</sup> Trade name.

<sup>(1)</sup> UNS numbers are listed in *Metals and Alloys in the Unified Numbering System*, published by the Society of Automotive Engineers (SAE International) and cosponsored by ASTM International.

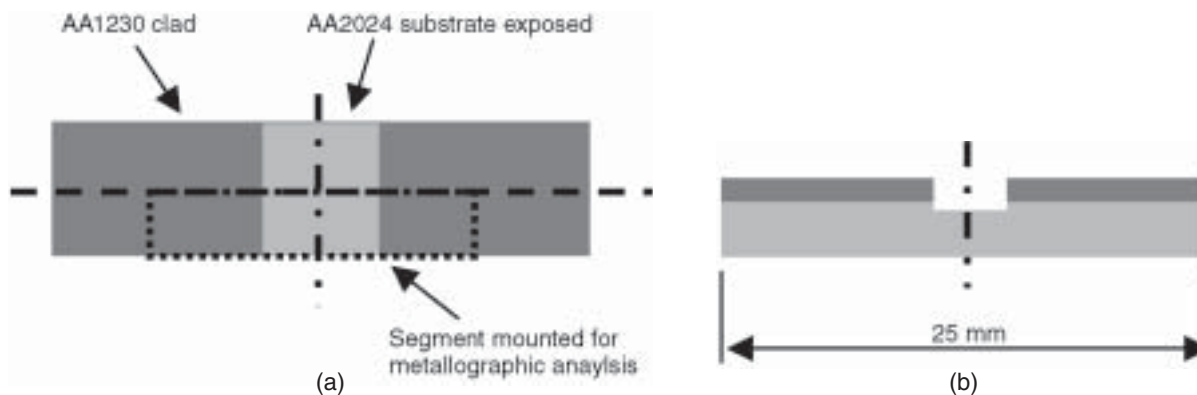


**FIGURE 1.** Schematic of specimen sectioning (not proportional). Specimens were first sectioned longitudinally along their centerline (dotted line); the lower halves were further trimmed on both ends to the edges of the dotted box. The upper halves were acid-cleaned for OM surface inspection. (a) Top view and (b) cross-sectional view of the segment.

The throwing power of Al cladding under realistic atmospheric conditions was thus investigated in this study by exposing Alclad AA2024-T3 with scratches of controlled size and geometry to an atmospheric marine environment at Daytona Beach, Florida. Coupons were removed after different exposure times and the damage was characterized. The results of metallographic examinations of the samples were complemented by computational modeling of the thin film exposure conditions using a computational code described in detail elsewhere.<sup>5</sup>

## EXPERIMENTAL PROCEDURES

### Specimen Description and Characterization Details

Alclad AA2024-T3 coupons with dimensions of 76 by 13 by 0.8 mm (3 by 1/2 by 1/32 in.) were used. The cladding consisted of ~50  $\mu\text{m}$  AA1230 (UNS A91230) on both sides. On all coupons, controlled scratches were made in the clad by using an end mill to machine away the cladding across the width of the coupons to make rectangular-shaped defects of varying widths (1, 2, 5, 6, 7, 8, 9, or 10 mm) at the center of the coupons. The exposures were performed by the Battelle Memorial Institute (Columbus, OH) at its Daytona Beach exposure site. The samples were located on racks at a position 75 m from the mean high tide. Digital photos were taken periodically to record the condition of the coupons. After 2, 4, 6, 12, and 18 months of exposure, selected coupons (one sample from each group) were removed for further characterization.<sup>6</sup>

All as-received specimens were first visually inspected and photographed. Specimens that had been exposed for 4, 12, and 18 months were selected for detailed investigation. As illustrated in Figure 1(a), these specimens were sectioned along their centerline (longitudinal direction), and one-half of each specimen was cleaned with acid (70% nitric acid [ $\text{HNO}_3$ ]

for 10 min) and then inspected under the optical microscope (OM). The other halves of these specimens were further trimmed to 2.5 cm (1 in.) wide with the scratch centered in the middle. The trimmed pieces (highlighted with a dotted box in Figure 1[a]) were then mounted in T-416<sup>†</sup> epoxy (Armstrong Epoxy Adhesives). To avoid the anomalous deposition at the edges and to ensure that the one-dimensional modeling was appropriate, cross sections close to the centerline (the cut) were exposed for metallographic analysis.

### Model Description

A computational mass-transport framework for occluded region corrosion<sup>7-9</sup> was extended to study the galvanic interactions of an Alclad layer with its Al alloy substrate in the vicinity of a scratch exposed to a thin electrolyte.<sup>10</sup> The model focuses on open-circuit conditions and local galvanic couples. The model outputs are potential and current distribution profiles along the length of the specimens. Based on the projected potential profiles and a protection potential criterion, percentages of protection corresponding to various scratch sizes were estimated. Both materials are assumed to have anodic passive regions limited by stable pitting at potentials above pitting potential ( $E_{\text{pit}}$ ) (varies with  $[\text{Cl}^-]$ ) and cathodic reactions dominating below corrosion potential ( $E_{\text{corr}}$ ) with both the pitting potential and the cathodic behavior determined by the alloy composition. Figure 2 shows the typical kinetic inputs, and a detailed description of this framework and post-data analysis are documented elsewhere.<sup>5</sup> Accurate electrochemical kinetics for Alclad and bare AA2024-T3 exposed to chloride solutions were used,<sup>11</sup> including the observed decrease in the pitting potential with increasing chloride concentration. The model was used to study the dependence of the throwing power on water layer thickness (WL), scratch size,  $[\text{Cl}^-]$ , passive current density ( $i_p$ ) of clad, and diffusion-limited current density ( $i_{\text{dl}}$ ) on the AA2024.

## RESULTS

In this section, the results of visual inspection of the as-received samples are first presented, followed by the optical microscope inspection of the cleaned surface, and metallographic analysis of the cross sections. For comparison, analyses of a set of bare AA2024 coupons exposed at the same site are also included. Finally, selected computational results are described in detail compared to the experimental observations.

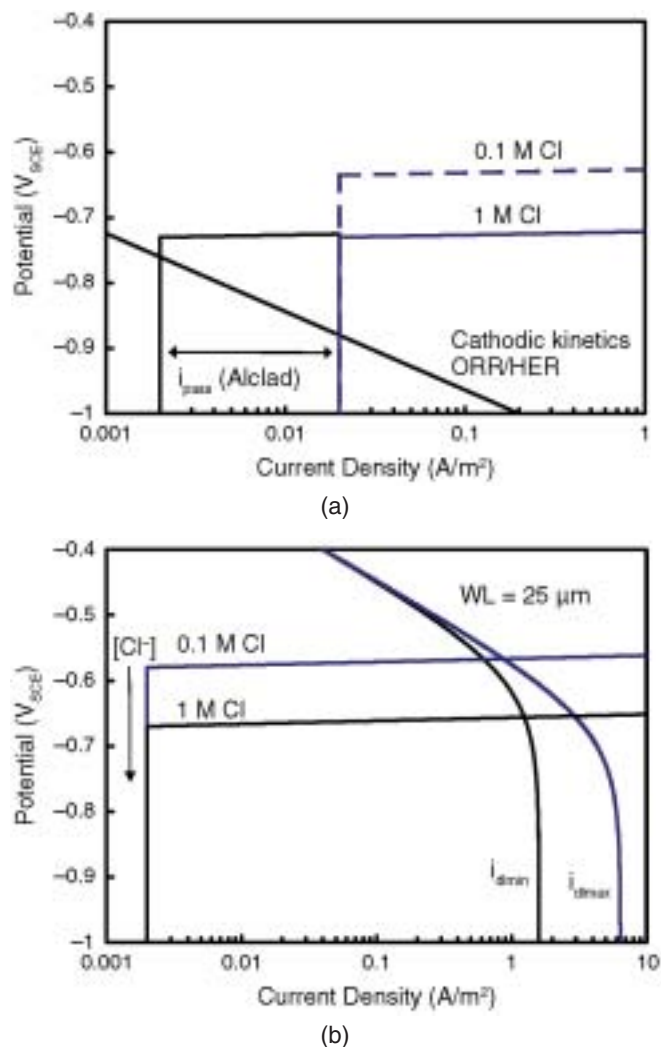
### Visual Inspection of As-Received Samples

Figure 3 shows the as-received surface appearance of selected coupons after exposure at DAB for various times, and Figure 4 presents higher magnification views of the scribed regions of all the coupons. As shown in both of the figures, after two months of exposure, the exposed AA2024-T3 of all the specimens with various widths was largely free of corrosion while the clad (especially the parts adjacent to the exposed AA2024-T3) already showed signs of corrosion. With increasing exposure time, the following features of surface condition development were observed:

- For a given scratch width, the amount of deposits on the exposed AA2024-T3 increased with time. Corrosion was often found in these areas by optical microscopy inspection after acid cleaning of the surface.
- The wider the scratch, the more deposits were formed on the exposed AA2024-T3. After 18 months of exposure, the specimen with a 10-mm scratch had a large number of deposits whereas most parts of the smaller scratches (5 mm or smaller) were still largely clean with only scattered deposits.
- For most of the specimens, one end of the scratch had more deposits than the other end; this is likely due to the orientation of the samples in the rack, which resulted in preferential deposits and aggregation of electrolytes at the bottom edge.
- Disregarding the anomalies close to the edge, the deposits on coupons tended to concentrate in the center of the scratches.
- The portions of the clad adjacent to the scratches had more deposits than the clad farther away from the scratches, with the amount of deposits appearing to increase with time as well.

### Optical Microscope Inspection of Cleaned Surfaces

Figure 5 shows the appearance of Alclad specimens with various scratch sizes after 12 months of exposure at DAB and subsequent cleaning. It is important to note that the pattern seen on the coupons is from machine marks left by the end mill that was



**FIGURE 2.** Kinetics input into the model: (a) Alclad and (b) AA2024 (for  $WL = 25 \mu m$ ). Also shown is the dependence of the  $E_{pit}$  values on  $[Cl^-]$ .

used to make the defects in the clad. Corrosion of specimens with 5-mm or smaller scratches was minor (isolated pits and in some cases a few corrosion clusters) and can be considered to have been largely protected (100% protection) by the clad. Conversely, the specimen with a 10-mm scratch corroded significantly with not only pits, but also zones of generalized corrosion connecting the pits. The parts close to clad, however, appear to have much less corrosion as a result of the protection provided by the clad. Similar features were observed on the specimens exposed for 18 months.

Another notable feature of the exposed AA2024-T3 is, as illustrated in Figure 6, that those specimens with scratches as small as 1 mm wide still had many shallow pits and a small number of larger, isolated pits. As discussed later in the Discussion section, these pits are likely caused by fluctuations in the water layer thickness during diurnal cycles.

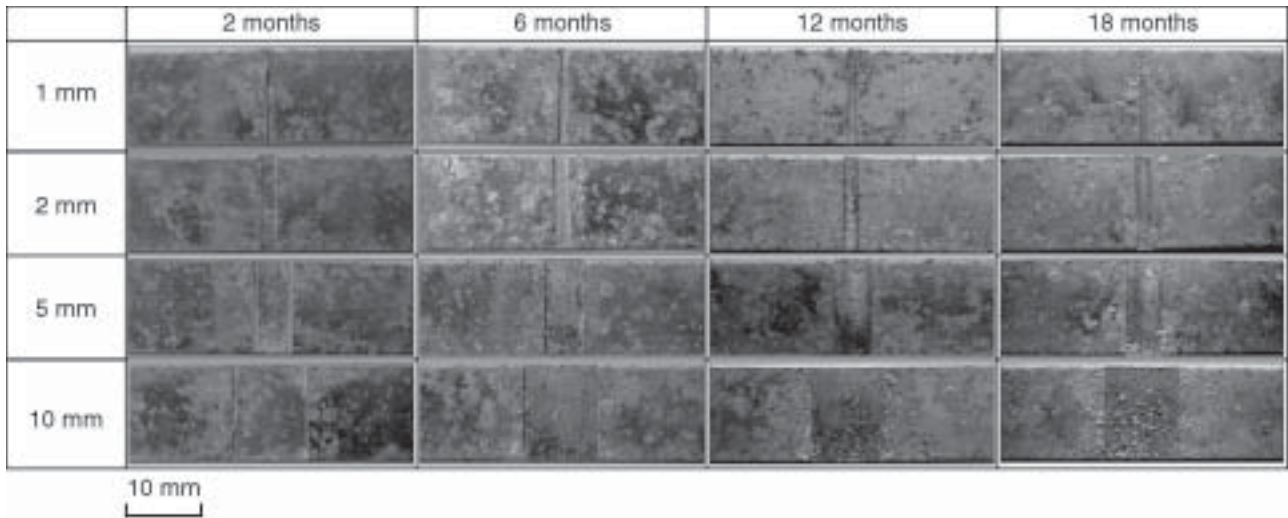


**FIGURE 3.** Surface conditions of scribed Alclad specimens after different exposure times at DAB. The amount of deposits/corrosion products on scratches increases with scratch size and exposure time and tends to concentrate in the middle of scratches. The Alclad adjacent to scratches experienced more corrosion than the Alclad farther away, and the amount of corrosion appears to increase with time as well.

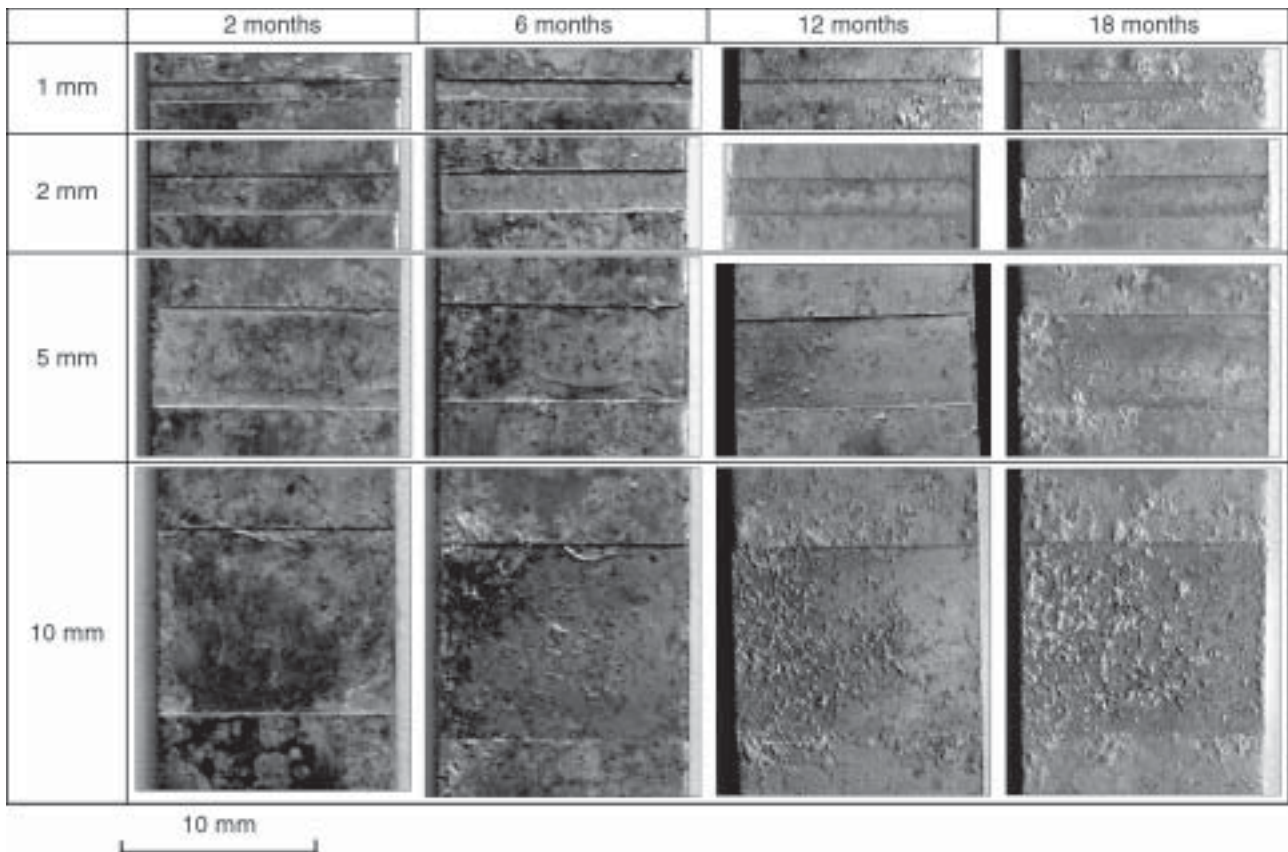


**FIGURE 4.** Surface conditions of the scribed Alclad specimens after different exposure times at DAB. Deposits/corrosion products on scratches increase with scratch size and exposure time and tend to concentrate in the middle of the scratches.

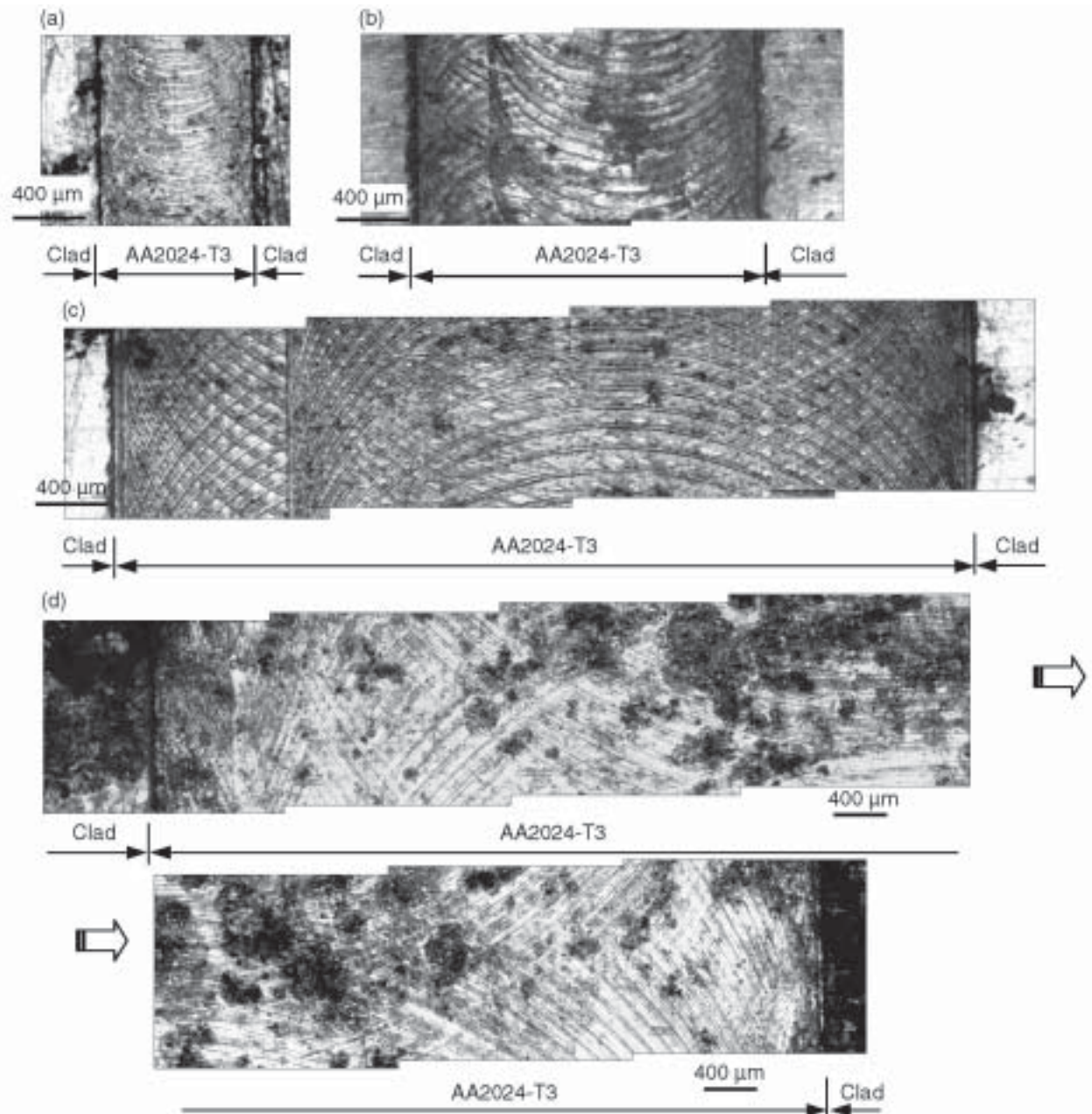


**FIGURE 5.** Surface conditions of Alclad specimens with various scratch sizes after 12 months' exposure at DAB: (a) 1 mm, (b) 2 mm, (c) 5 mm, and (d) 10 mm. Coupons with 5-mm or smaller scratches had only moderate or minor corrosion (roughly 100% protection), whereas the one with the 10-mm scratch was corroded significantly in the middle of the scratch. The pattern seen on the coupons is from machine marks left by the end mill used to make the scratches. The black areas are the corroded regions.

While the coupons with 5-mm or smaller scratches were 100% protected, the percentage of the scratch area protected for the larger scratches was estimated to quantify the throwing power of the cladding. To minimize the interference from the diurnal cycle-induced corrosion, two approaches were used:

- Coupons exposed for a shorter time (4 months) were used.
- A protection range was estimated for each scratch size.

The range was estimated in two ways to bracket the extent of damage:

*Minimal protection*—the area protected assuming minimal diurnal cycle-induced corrosion (i.e., all corrosion was caused by the limited clad throwing power except some isolated pits close to the clad edges).

*Maximum protection*—the area protected assuming significant diurnal cycle-induced corrosion (i.e., the intermediate areas with moderate attack were attributed to diurnal cycles).

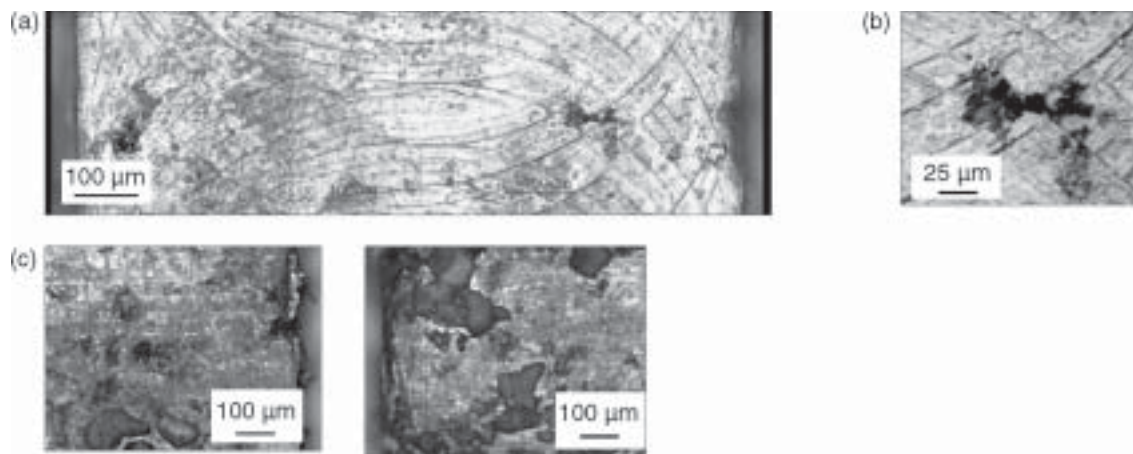


**FIGURE 6.** Surface condition of Alclad specimens with a 1-mm scratch after 18 months' exposure at DAB (~3.5 mm to the upper edge): (a) overall view of the exposed AA2024-T3, which has many scattered shallow pits and a few significant isolated pits likely due to diurnal cycling; (b) a significant pit (~0.2 mm to the right edge); (c) condition of AA1230 cladding next to the scratch that was heavily corroded although not uniform. The pattern seen on the coupon is from machine marks left by the end mill used to make the scratches. The black areas are the corroded regions.

Although the determination of "significant diurnal cycle-induced corrosion" can be rather subjective, it was determined in such a way that the estimated corresponding protection was always 20% higher than that estimated by assuming minimal diurnal-induced corrosion.

The estimated protection ranges of these coupons are graphically shown in Figure 7 using two different types of bars (grid bar for minimal protection and solid bar for maximum protection). Considering the symmetric nature of the scratch surfaces, only approximately half of each scratch is presented. Figure 7 shows that, for all the scribed coupons, the regions adjacent to Al clad were well-protected while the parts in the center of the scratches were moderately (6-mm to 9-mm scratches) or significantly (10-mm scratch) attacked.

In summary, the following observations were made from the OM inspection of the cleaned surfaces:

- Scratches of 5 mm or less in width were generally protected by clad, while scratches between 6 mm and 10 mm wide were only partially protected.
- Even scratches well protected by the clad were still subject to isolated pitting corrosion.

The OM inspection also shows (Figure 6) that the AA1230 cladding closest to the scratches suffered severe corrosion. In fact, the corrosion of this region of cladding was more severe than that in the scratches, as illustrated in Figures 8 and 9, and much more severe than the areas of the cladding farther away from the scratch (Figure 3).

### Metallographic Analysis

**12-Month Exposures** — Figure 8 shows a series of cross-sectional views of a specimen with a 5-mm

scratch exposed at DAB for 12 months that well represents the behavior of all specimens with smaller scratches. The exposed AA2024-T3 was largely unattacked. This figure also shows that some parts of the clad (i.e., Point 4) experienced significant pitting corrosion, which, in some areas, almost penetrated the entire thickness of clad AA1230. In agreement with the OM analysis, the overall corrosion of specimens with 5-mm or smaller scratches was minor and the exposed AA2024-T3 can be considered to have been protected by the clad.

As shown in Figure 9, a 10-mm scratch experienced significant corrosion after 12 months of exposure. A significant pit (Point 5 in Figure 9) was observed (~20  $\mu\text{m}$  deep and about 3.8 mm away from the clad to the right). It is also evident that corrosion tended to concentrate in the middle of the scratch while the areas of the substrate close to the clad were well protected. It is noted that in the as-received condition, the entire AA2024-T3 region was often covered with deposits, although the underlying AA2024-T3 was found to have not suffered corrosion (as evidenced by Point 6). These deposits could have been salt deposits from the atmosphere and/or corrosion products formed elsewhere, but transported by wind or rain action. Upon acidic cleaning, these deposits were easily removed.

**18-Month Exposures** — The 18-month exposure samples shown in Figures 10 and 11 are qualitatively similar to the 12-month samples, although the extent of corrosion increased. After 18 months of exposure, the exposed AA2024-T3 of specimens with 5-mm (Figure 10) or smaller scratches were largely free of corrosion, although some parts were occasionally covered with deposits. The specimen with the 10-mm scratch, however, experienced more severe corrosion than was

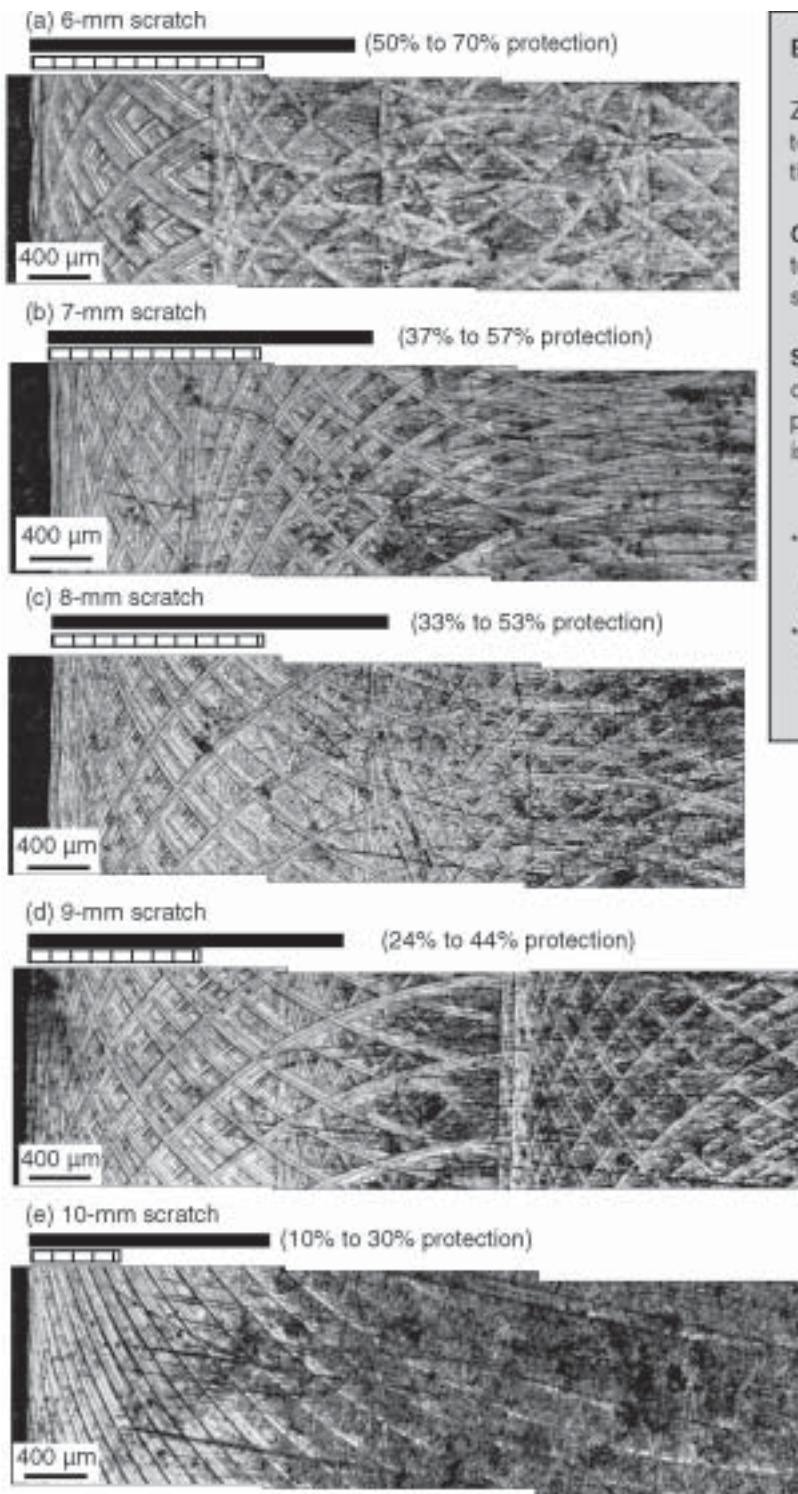


**FIGURE 7.** Surface condition of Alclad specimens with various scratch sizes after 4 months' exposure. Considering the symmetric nature of the scratch surfaces, only about half of each scratch is presented. The black stains are the result of corrosion, and the clad is out of each picture to the left.

#### Bars used to illustrate protection range

Zones under the bars are protected (clad is to the left of pictures). Zones to the right of the bars suffered corrosion.

**Grid bar:** Assumes minimal corrosion due to diurnal cycles, region indicated by bar showed virtually no corrosion.

**Solid bar:** Assumes considerable corrosion due to diurnal cycles; thus, it includes the portion of the surface that may have been isolated at times and showed scattered pits.

\* The patterns seen on the coupon are machining marks left by the end mill used to make the scratches.

\* The black areas are typically corroded regions.

observed at 12 months. Both pitting and intergranular corrosion, as shown in Figure 11, were observed. The numbers in Figure 11 indicate a variety of locations of interest. Points 1, 2, and 22 through 24 were

not attacked, whereas the other points all showed different levels of attack. As for the 12-month sample, corrosion was more frequent near the middle whereas areas close to the clad were largely protected.

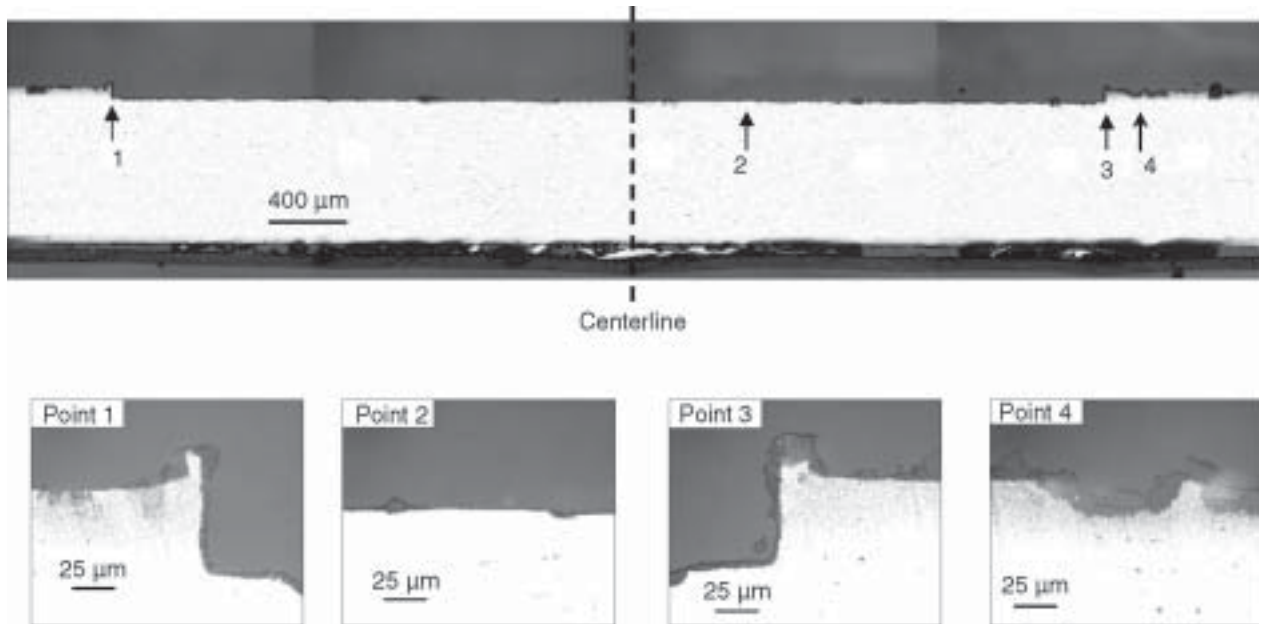


**FIGURE 8.** Cross-sectional photomicrograph of Alclad specimen with a 5-mm scratch after 12 months' exposure at DAB. The exposed AA2024 was largely unattacked. (Point 2 is about 3.2 mm from the left edge; Point 4 is about 0.2 mm from the right edge.)

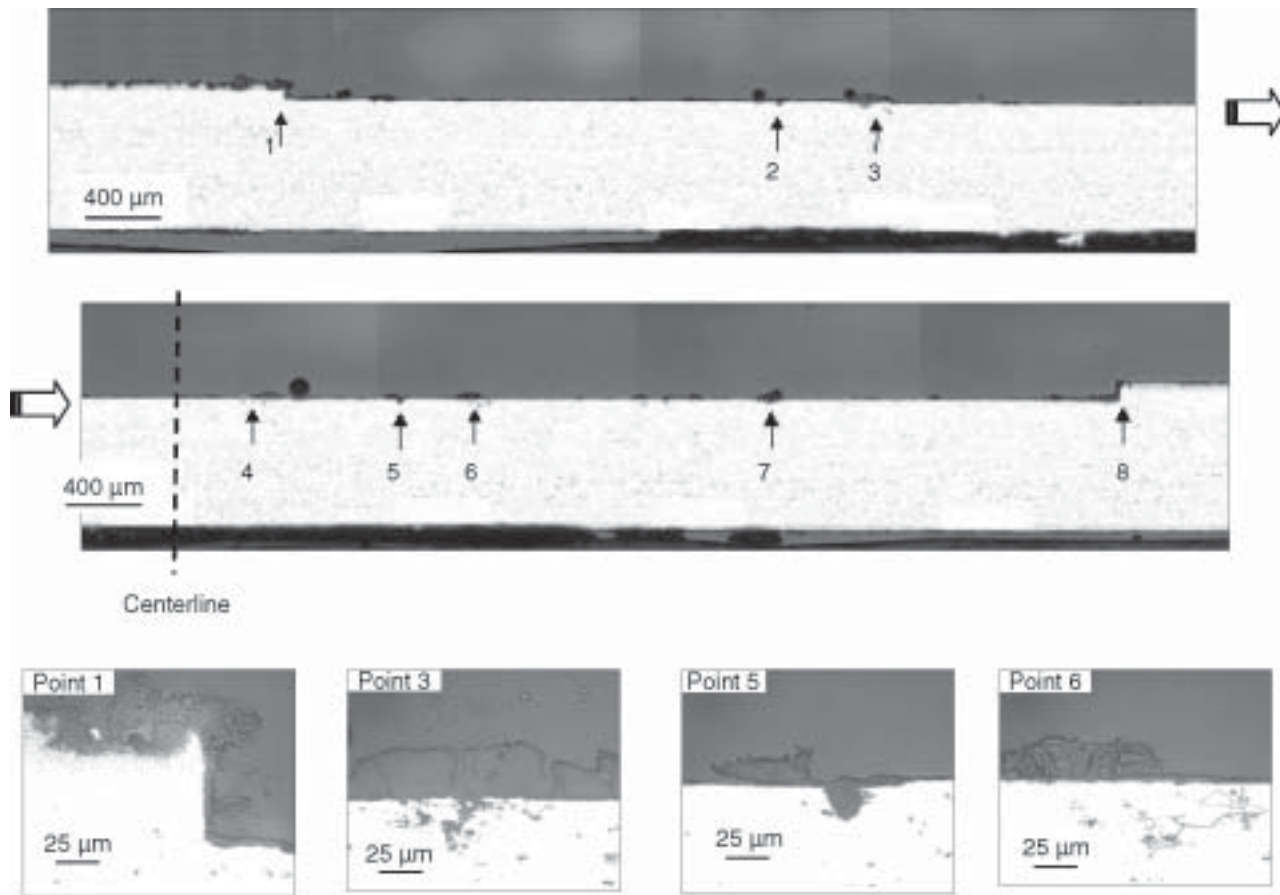


**FIGURE 9.** Cross-sectional photomicrograph of Alclad specimen with a 10-mm scratch after 12 months' exposure at DAB. Significant corrosion was observed in the middle of the scratch while regions close to Alclad were largely free of corrosion. (Position of selected points, distance from the left edge of scratch: Point 3, ~3.0 mm; Point 5, ~6.2 mm; Point 6, ~6.7 mm.)

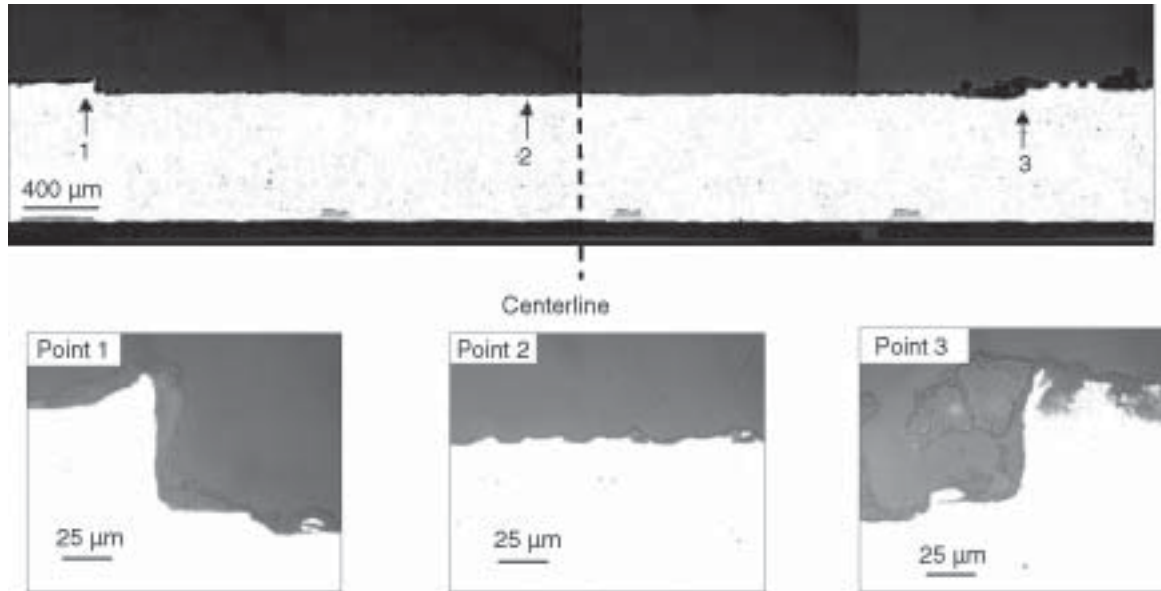


**FIGURE 10.** Cross-sectional photomicrograph of Alclad specimen with a 5 mm-wide scratch after 18 months' exposure at DAB. The exposed AA2024 was largely free of corrosion. (Position of Point 2: ~2.3 mm from the left edge of scratch.)

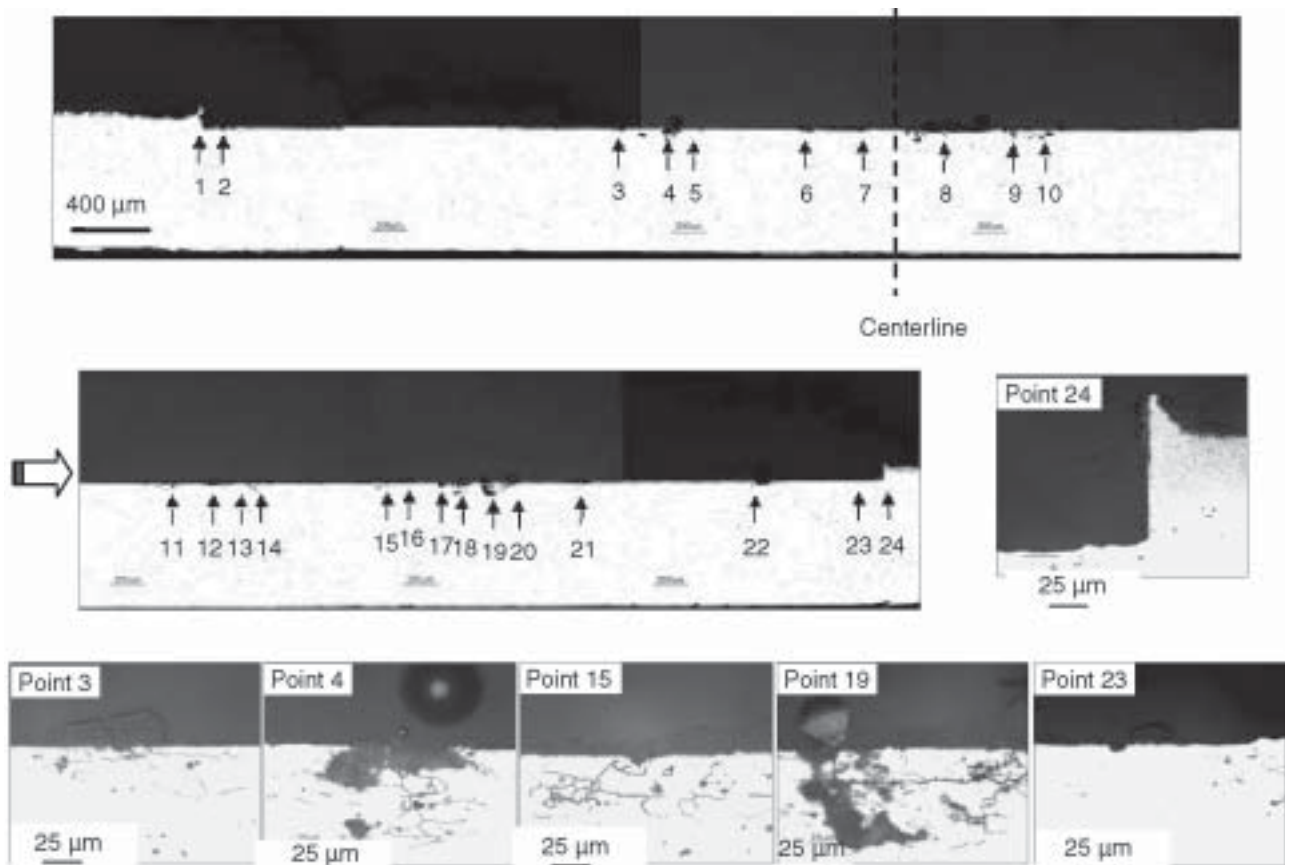


**FIGURE 11.** Cross-sectional photomicrograph of Alclad specimen with a 10-mm scratch after 18 months' exposure at DAB. Significant corrosion was observed in the middle of the scratch while regions close to Alclad were largely free of corrosion. (Position of selected points, distance from the left edge of the scratch: Point 4, ~2.6 mm; Point 15, 7.2 mm; Point 19, 7.9 mm.)

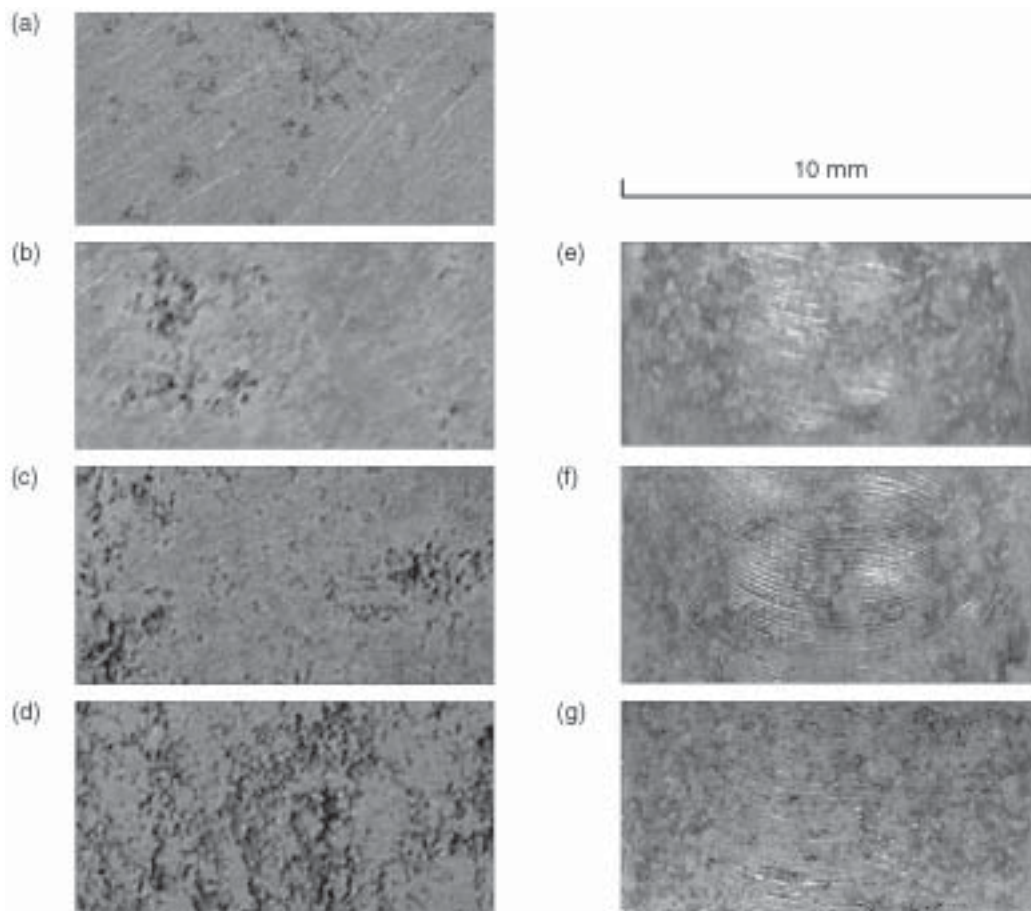


**FIGURE 12.** Surface condition of bare AA2024 compared with scribed Alclad AA2024 (all specimens were acid-cleaned). Bare AA2024 exposed after: (a) 4 months, (b) 6 months, (c) 12 months, and (d) 2 years. Scribed Alclad AA2024 with 10-mm scratches exposed after: (e) 6 months, (f) 12 months, and (g) 18 months. Corrosion of bare AA2024 is evidently more severe than scribed Alclad coupons. (For each coupon, only a representative portion of 10 mm by 5 mm was presented for comparison.)

For comparison, a set of bare AA2024-T3 coupons (45 by 17 by 0.6 mm) that were exposed at DAB for 3, 6, 12, and 24 months were also analyzed. These coupons were acid cleaned before shipping.<sup>12</sup> Figure 12 compares the surface condition of bare AA2024 and scribed Alclad AA2024 for different exposure times. As expected, bare AA2024 experienced much more severe corrosion than those scribed Alclad coupons. Bare AA2024 coupons, for example, exhibited widespread corrosion after only two months of exposure (Figure 12[a]) and extensive attack after twelve months' or longer exposure (Figures 12[c] and [d]). Figure 13 shows two selected cross-sectional images of areas of bare AA2024-T3 after 12 months' exposure, in which corrosion in one case had penetrated two-thirds of the thickness of the coupon (~0.6 mm). Even the 10-mm scribed specimens, in contrast, only exhibited an ~20- $\mu\text{m}$ -deep pit (shown in Figure 9) after the same exposure period. This observation thus confirmed the protection effect of AA1230 cladding, even when protection is not complete.

### Computational Modeling

Figure 14 shows the calculated percentage of the AA2024-T3 scratch protected as a function of scratch width for a range of parameters, as well as the averages of the estimated protection ranges for coupons exposed at DAB for 4 months together with  $\pm 10\%$  error bars. The data point corresponding to 100% protection of a 5-mm scratch was based on observations from specimens exposed for one year described earlier. Although a wide range of input parameter combinations (2 levels for WL and [Cl], 2 levels for  $i_p$  and  $i_{dl}$ ) was tested, only one set of computations accurately predicted the experimentally observed trend of protection with increasing scratch sizes: [Cl] = 1 M, WL = 25  $\mu\text{m}$ ,  $i_p = 0.002 \text{ A/m}^2$ ,  $i_{dl} = 1.6 \text{ A/m}^2$ .

Figure 14 also illustrates the effect of [Cl],  $i_p$ ,  $i_{dl}$ , and WL. Using the case of [Cl] = 1 M, WL = 25  $\mu\text{m}$ ,  $i_p = 0.002 \text{ A/m}^2$ , and  $i_{dl} = 1.6 \text{ A/m}^2$  (empty squares as shown) as reference, the qualitative effect of the parameters can be seen. The protection provided by the clad significantly decreased when [Cl] was decreased

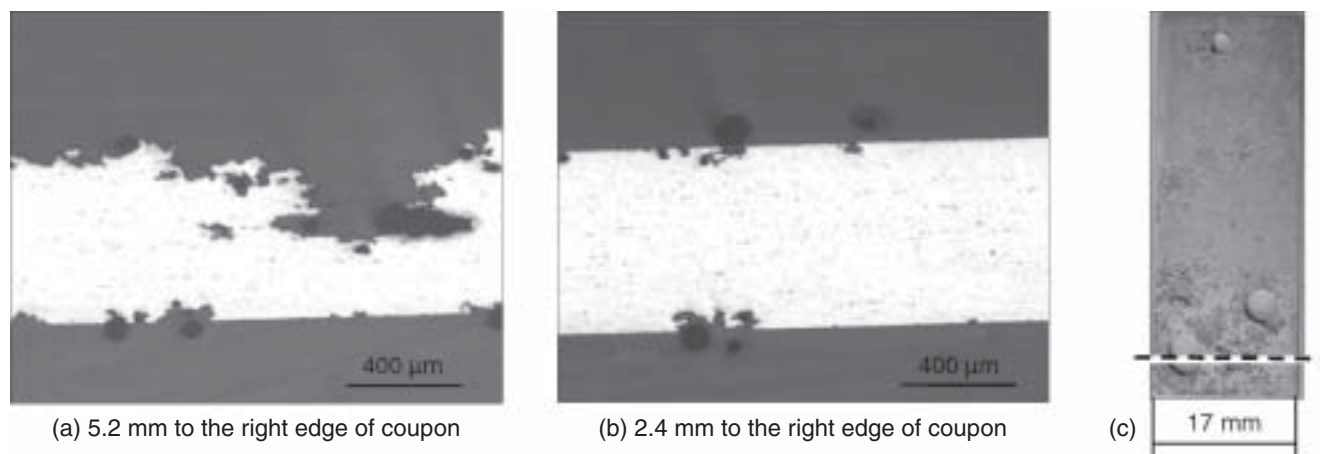


**FIGURE 13.** Cross-sectional photomicrograph of bare AA2024-T3 after 12 months' exposure at DAB. (a) Corrosion in one case had penetrated as far as 2/3 of the whole coupon thickness. The bare AA2024 exposed at DAB for 12 months was sectioned along the dotted line as shown in (c), and the lower part was mounted for cross-sectional examination.

from 1 M to 0.5 M (filled diamonds). This effect is as expected as lower  $[Cl^-]$  reduced the conductivity of the surface electrolyte. The case with the larger  $i_{dl}$  ( $6.4 \text{ A/m}^2$ ) (the empty circles) represents a situation in which the cathodic reaction rate is enlarged, for example, when Cu replating has taken place. Under these circumstances the clad provided less protection: only 24% protection for the 5-mm scratch ( $S = 2.5 \text{ mm}$ ) and 10.5% for the 10-mm scratch. The case with the larger  $i_p$  ( $0.02 \text{ A/m}^2$ ) (filled triangles) projected a mildly higher protection, i.e., 25% for the 10-mm scratch. The predicted protection for the control case with  $i_p = 0.002 \text{ A/m}^2$  was 20.9%. When the WL was increased from  $25 \mu\text{m}$  to  $100 \mu\text{m}$ , the calculation projected that the clad could provide full protection for scratches up to 10 mm, suggesting a significant positive effect of WL. A detailed summary of computational results of these cases is provided in Table 1, showing that all these parameters have a significant impact on the throwing power of the cladding.

## DISCUSSION

Metallic claddings have a long and successful history of protecting structural materials. The development and implementation of Al clads for precipitation-hardened aluminum alloy is responsible for the greatly improved corrosion performance of aircraft structures using sheet product. Sacrificial cathodic protection has been widely studied both experimentally<sup>13-14</sup> and computationally<sup>15-16</sup> for conditions of full immersion in electrolytes, including soil. The state of the art allows the efficient design of sacrificial cathodic protection systems via optimal placement of immersed anodes. The situation is substantially different for materials exposed to atmospheric conditions in which a thin electrolyte layer develops. Whereas there have been many outdoor exposures at seacoast

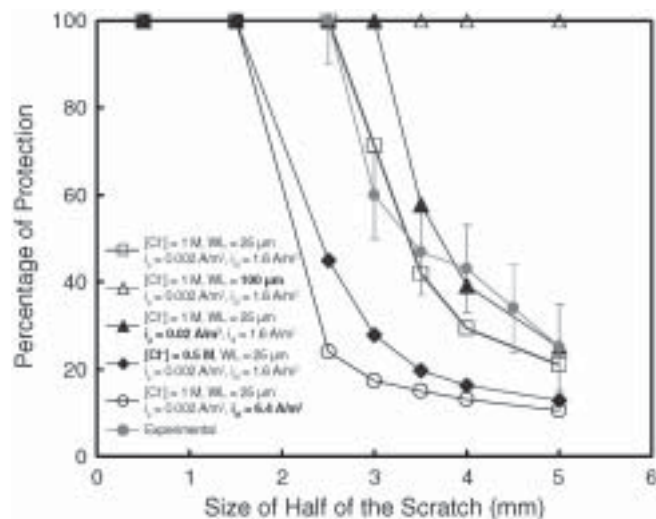


**FIGURE 14.** Calculated percentage of protection as a function of scratch width for a range of parameters, compared with the experimental observation. The case with  $[Cl^-] = 1 \text{ M}$ ,  $WL = 25 \mu\text{m}$ ,  $i_p = 0.002 \text{ A/m}^2$ , and  $i_{dl} = 1.6 \text{ A/m}^2$  best fits the experimental observation. ( $0.01 \text{ A/m}^2 = 1 \mu\text{A/cm}^2$ ).

**TABLE 1**  
Effect of Various Parameters  
on Throwing Power of Alclad<sup>†</sup>

Parameters	Size of Scratch (2S, mm)		
	5	8	10
	Percentage of the exposed AA2024 protected		
Base case <sup>(A)</sup>	100	29.4	20.9
Lower $[Cl^-]$ : <sup>(B)</sup> 0.5 M	45	16.2	12.9
Higher $i_p$ : <sup>(B)</sup> $0.02 \text{ A/m}^2$	100	39.2	25
Higher $i_{dl}$ : <sup>(B)</sup> $6.4 \text{ A/m}^2$	24	13.1	10.5
Higher WL: <sup>(B)</sup> $100 \mu\text{m}$	100	100	100

<sup>(A)</sup> Base case:  $[Cl^-] = 1 \text{ M}$ ,  $WL = 25 \mu\text{m}$ ,  $i_p = 0.002 \text{ A/m}^2$ ,  $i_{dl} = 1.6 \text{ A/m}^2$ .

<sup>(B)</sup> The only parameter changed compared to the base case.

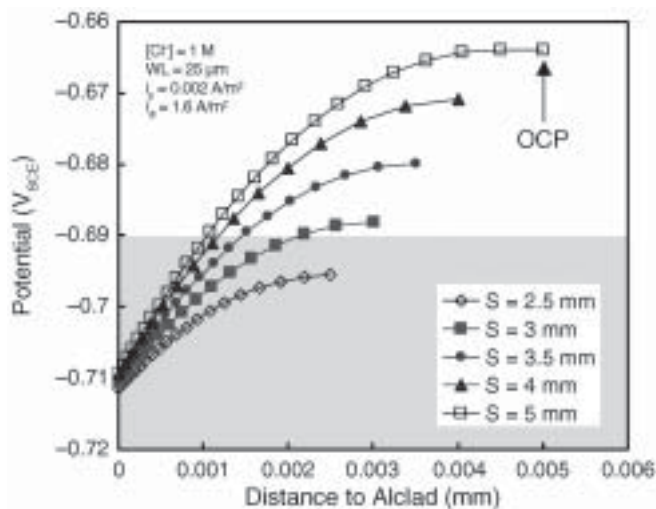


**FIGURE 15.** Potential profiles of scratched AA2024-T3 for a selected case.  $S$  is the size of the half scratch. Based on a protection criterion that  $E < -0.69$  V, the parts in the gray region are protected by the Alclad. With increased scratch size, the potential profile changes and the potential at the scratch center (last point of each curve) gradually approaches the OCP of the alloy. Once this value is reached ( $S = 5$  mm), the potential profile stabilizes, suggesting a constant protection area  $X_{\text{prot}}$  for larger scratches ( $S \geq 5$  mm). For scratches 3, 3.5, and 4 mm,  $X_{\text{prot}}$  decreases with scratch size; for scratches 2.5 mm or smaller,  $X_{\text{prot}} = 2 \times S$ .

and other sites of clad material as well as laboratory exposures, little quantitative information is available regarding the throwing power of clads under thin film conditions. Computational studies of corrosion in thin electrolytes have been limited to material couples whose individual components exhibit electrochemical kinetics that obey the linear or Tafel relation.<sup>17-19</sup> Neither Alclad nor AA2024-T3 exhibit linear or Tafel behavior in either their anodic or cathodic kinetics.

Figures 12 and 13 clearly demonstrate the benefits of Al cladding. The bare AA2024-T3 was severely attacked during exposure to the aggressive seacoast environment, suffering extensive pitting, in some areas removing  $\sim 0.4$  mm (ca. 2/3) of the material thickness. For the conditions tested here, scratches below 5 mm in width can be completely protected for long periods of time ( $>18$  months) by Alclad. The small pits scattered over the surface in these specimens are most likely due to fluctuations in the water layer thickness during diurnal cycles. During times of drying, the solution layer thinned until electrolytic contact was lost between the clad and the AA2024-T3. At that point, isolated solution droplets formed on the surface, decoupling areas within the scratch from the cladding. The limited size of the pits (typically a few microns or less) supports the idea that they do not grow for long and do not have a large cathodic area available to support their growth.

Although small scratches (5 mm or smaller) enjoy full protection from the clad, larger scratches were

only partially protected. For example, the 10-mm scratch suffered extensive pitting and intergranular corrosion, with the damage being observable quite quickly (4 months). Under this condition, only 10% to 30% of the scratch nearest the clad was protected. The scratch area farther away from the clad exhibited corrosion that grew over the entire 1.5-year exposure period. This focusing of the attack near the center of the scratch is as expected, but this work represents one of the few systematic, quantitative measurements of the extent of the protection available in the open literature. The observation of intergranular corrosion (Figure 11) implies that either the potential of the scratch was reasonably high, as intergranular corrosion is observed at elevated potentials in potentiodynamic scans,<sup>20-21</sup> or that a concentrated chloride solution with substantial acidity was present.<sup>22</sup>

Interestingly, the empirical equation obtained from the data fitting suggests a simple relation between scratch size ( $2 \times S$ ,  $5 \text{ mm} \geq S > 2.5 \text{ mm}$ ) and percentage of protection ( $y$ ):

$$y = 620 \times S^{-2} \quad (1)$$

where  $S$  is the size of half of a scratch, and the units of  $S$  and  $y$  are mm and %, respectively. When  $S$  is 2.5 mm or smaller,  $y = 100$  %. The actual length of the protected scratch  $X_{\text{prot}}$  ( $y \times 2S$ ) thus increases linearly with the inverse of  $S$ :

$$X_{\text{prot}} = 12.4 / S (5 \text{ mm} \geq S > 2.5 \text{ mm}) \quad (2)$$

This relation does not correspond to the known crevice corrosion scaling law,<sup>7-8,23-25</sup> as might be expected because of the similarity in mass transport. To explore the possible origin of this deviation, potential profiles of several scratches for the case that best predicts this experimental observation were plotted in Figure 15 ( $[Cl^-] = 1 \text{ M}$ ,  $WL = 25 \mu\text{m}$ ,  $i_p = 0.002 \text{ A/m}^2$ ,  $i_{cl} = 1.6 \text{ A/m}^2$ ). Apparently, as the scratch size ( $2S$ ) increases, the potential at the scratch center (last point to the right of each curve) gradually approaches the open-circuit potential (OCP) of AA2024-T3. When  $S = 5$  mm, for this particular case, the potential profile stabilized and will not change with a further increase of scratch size because the OCP has been reached. Given a chosen protection criteria, e.g.,  $-0.69$  V,  $X_{\text{prot}}$  can be divided into three zones of interest based on the length of scratches:

- small scratches (i.e.,  $S < \sim 3$  mm for this particular case),  $X_{\text{prot}} = 2 \times S$
- intermediate scratches (i.e.,  $\sim 3 \text{ mm} < S < 5 \text{ mm}$ ),  $X_{\text{prot}}$  decreases with scratch size and the trend can largely be described by Equation (2)
- large scratches (i.e.,  $S \geq 5 \text{ mm}$ ),  $X_{\text{prot}}$  is a constant that would thus satisfy the scaling law

An inherent assumption in scaling laws is that the bounding potentials (i.e., at the center of the scratch

and at the far end of the clad) remain constant. This issue will be further addressed in a future report.

Modeling of atmospheric exposures is extremely challenging due to the transient nature of the environmental conditions. Nonetheless, insights can be gained by determining what sets of steady-state conditions would result in the distribution of the attack observed. Because of the complex and highly nonlinear electrochemical kinetics used, the development of solutions based on nondimensionalized parameters is not possible. The fact that the higher chloride concentration (1 M) with the small WL (25  $\mu\text{m}$ ) best describes the experimental data might suggest that the WL present in the field is of that order. It is important to note that the model assumes a constant water layer and considers an instantaneous coupling, whereas the field tests surely were subject to oscillations on the WL. Nonetheless, the agreement between independent experimental and computational results implies that the protection ability of metallic claddings can be predicted computationally.

## CONCLUSIONS

- ❖ For scratches 5 mm wide or smaller, the exposed AA2024-T3 was generally well protected by Alclad.
- ❖ For scratches larger than 5 mm, the percentage of protection decreased with increasing scratch size according to a simple quadratic equation.
- ❖ In all cases, Alclad experienced the most severe corrosion near the clad/scratch junction.
- ❖ Besides corrosion within the scribes due to the limited throwing power of the clad, scattered pitting corrosion within the scribes was observed due to diurnal cycles of wet-dry cycling, which led to islands of solution on the substrate ionically isolated from the clad.
- ❖ Computation shows that WL, scratch size,  $[\text{Cl}^-]$ ,  $i_p$  of clad, and  $i_{\text{dl}}$  of AA2024 all have a significant impact on the throwing power of clad.
- ❖ Modeling calculations produce comparable results to experimental observation using reasonable input parameters ( $[\text{Cl}^-] = 1 \text{ M}$ ,  $\text{WL} = 25 \mu\text{m}$ ,  $i_p = 0.002 \text{ A/m}^2$ , and  $i_{\text{dl}} = 1.6 \text{ A/m}^2$ ).

## ACKNOWLEDGMENTS

W.H. Abbott (Battelle Columbus) is gratefully acknowledged for the provision of the samples that were tested as part of the United States Air Force (USAF) Air Vehicle Health Management Program, Maj. T. Harigton (AAA/ASC).

## REFERENCES

1. R.H. Brown, "Aluminum Alloy Laminates-Alclad and Clad Aluminum Alloy Products," a chapter in *Engineering Laminates*, ed. A.G. Dietz (Cambridge, MA: MIT Press, 1969), p. 227.
2. W.W. Binger, "Aluminum and Its Alloys," in *Corrosion Resistance of Metals and Alloys*, 2nd ed., eds. F.L. LaQue, H.R. Copson (New York, NY: Reinhold Publishing Corp., 1963), p. 192.
3. E.H. Dix, "Alclad—A New Corrosion Resistant Aluminum Product," National Advisory Committee Technical Note, August 1927.
4. C.J. Walton, D.O. Sprowls, J.A. Nock, Jr., *Corrosion* 9 (1953): p. 345.
5. F. Presuel-Moreno, F. Cui, R.G. Kelly, "Modeling of Corrosion Protection Provided by an Aluminum-Based Clad: Water Layer Effect," in *Corrosion and Protection of Light Metal Alloys*, eds. R.G. Buchheit, R.G. Kelly, N.A. Missert, B.A. Shaw, PV 2003-23 (Pennington, NJ: The Electrochemical Society, Inc., 2004), p. 344.
6. W.H. Abbott, "Monthly Status Report on Corrosion Effects on Structural Integrity," Subcontract no. F0965-00-D-0018-0001, Battelle, September 2002.
7. J.S. Lee, M.L. Reed, R.G. Kelly, *J. Electrochem. Soc.* 151, 7 (2004): p. B423.
8. L.A. DeJong, R.G. Kelly, "The Demonstration of the Microfabrication of Rigorously Defined Crevices for the Investigation of Crevice Corrosion Scaling Laws," in *Critical Factors in Localized Corrosion III*, eds. R.G. Kelly, G.S. Frankel, P.M. Natisian, R.C. Newman, PV 98-17 (Pennington, NJ: The Electrochemical Society, Inc., 1999), p. 678.
9. R.G. Kelly, K.C. Stewart, "Combining the Ohmic Drop and Critical Crevice Solution Approaches to Rationalize Intermediate Attack in Crevice Corrosion," in *Passivity of Metals and Semiconductors VIII*, eds. M.B. Ives, B.R. MacDougall, J.A. Bardwell, PV 99-42 (Pennington, NJ: The Electrochemical Society, 1999), p. 546.
10. H. Wang, F. Preseul, R.G. Kelly, *Electrochim. Acta* 49, 2 (2004): p. 239.
11. S.T. Pride, J.R. Scully, J.L. Hudson, "Analysis of Electrochemical Noise from Metastable Pitting in Aluminum, Aged Al-2%Cu, and AA 2024-T3," in *Electrochemical Noise Measurements for Corrosion Applications*, ASTM STP 1277, eds. J.R. Kearns, J.R. Scully, P.R. Roberge, D.L. Reichert, J.L. Dawson (West Conshohocken, PA: ASTM International, 1996), p. 307.
12. Private communication to W.H. Abbott, Battelle.
13. T. Banerjee, G. Mishra, *J. Metall. Mater. Sci.* 42, 3 (2000): p. 167.
14. V. Ashworth, C. Googan, *Cathodic Protection: Theory and Practice* (Leighton Buzzard, Bedfordshire, U.K.: The Institute of Corrosion, 1993).
15. D. Rabiot, F. Dalard, J.J. Rameau, J.P. Caire, S. Boyer, *J. Appl. Electrochem.* 29, 5 (1999): p. 541.
16. F.J. Presuel-Moreno, M.E. Goldman, R.G. Kelly, J.R. Scully, "Electrochemical Sacrificial Cathodic Prevention Provided by a Al-Co-Ce Metal Coating Coupled to A2024-T3," in *Corrosion and Protection of Light Metal Alloys*, eds. R.G. Buchheit, R.G. Kelly, N.A. Missert, B.A. Shaw, PV 2003-23 (Pennington, NJ: The Electrochemical Society, Inc., 2004), p. 255.
17. J.T. Waber, B. Fagan, *J. Electrochem. Soc.* 103 (1956): p. 64-72.
18. E. McCafferty, *J. Electrochem. Soc.* 124 (1978): p. 1,869.
19. R. Morris, W. Smyrl, *J. Electrochem. Soc.* 136, 11 (1989): p. 3,229.
20. W. Zhang, G.S. Frankel, *Electrochim. Acta* 48, 9 (2003): p. 1,193.
21. V. Guillaumin, G. Mankowski, *Corros. Sci.* 41, 3 (1999): p. 421.
22. J.R. Scully, "Intergranular Corrosion," in *Encyclopedia of Electrochemistry*, vol. 4, *Corrosion and Oxide Films*, eds. A.J. Bard, M. Stratmann, G.S. Frankel (Weinheim, Germany: Wiley-VCH, 2003), p. 344.
23. A. Turnbull, J.G.N. Thomas, *J. Electrochem. Soc.* 129 (1982): p. 1,412.
24. M.J. Psaila-Dombrowski, "Modeling of Crack and Crevice Chemistry in Light Water Environments" (Ph.D. diss., Department of Materials Science and Engineering, Massachusetts Institute of Technology, 1990).
25. Y. Xu, H.W. Pickering, *J. Electrochem. Soc.* 140 (1993): p. 658.